ADVANCED INTELLIGENT SYSTEMS Open Access
www.advintellsyst.com

Spatiotemporally Controlled Soft Robotics with Optically Responsive Liquid Crystal Elastomers

*Elizabeth R. Blackert, Phoebe Scaccia, Morgan Barnes, Taniya M. S. K. Pathiranage, Rafael Verduzco, Vaibhav Unhelkar, and Hanyu Zhu**

Light-responsive materials enable the development of soft robots that are controlled remotely in 3D space and time without the need for cumbersome wires, onboard batteries, or altering the local environment. Azobenzene liquid crystal polymer networks are one such material that can move and deform in response to light actuation. Previous works have demonstrated azo-based soft robotic grippers and transporters that are remotely powered by light. However, highly adaptive, automated spatiotemporal optical control over these materials has not yet been realized. Herein, a system for an azobenzene liquid crystal elastomer soft robotic arm is created by dynamically patterning light for independently maneuverable joints. The nonlinear material response to optical actuation is characterized, and the broad actuation space is explored with diverse arm configurations. A neural network is trained on the arm configurations and corresponding laser pattern to automate the pattern generation for a desired configuration. Finally, the azobenzene liquid crystal elastomer arm demonstrates complex targeted motion, marking an important step toward optically actuated soft robotics with applications ranging from optomechanics to biomedical tools.

1. Introduction

Azobenzene liquid crystal polymer networks (azoLCNs) have received significant research interest in recent years due to their ability to move and deform in response to light.[1–7] Light is an optimal stimulus for remote energy delivery and contactless control with high spatiotemporal precision. Stimuli-responsive liquid crystal polymers are composed of long, rod-like liquid crystalline molecules that align with each other, granting orientational order to the polymer network. Azobenzene is a photochromic molecule that is highly absorptive in the UV–vis light range.[1] Upon absorption of a photon, a combination of azobenzene isomerization and local heating within the network disrupts the liquid crystalline alignment, causing macroscopic deformation.[8,9] This photomechanical response has been shown to be reversible,[1] rapid,[10,11] and repeatable up to thousands of times.[12] Interestingly, even uniformly aligned materials with simple geometry can enable nontrivial self-regulated dynamics under constant illumination.[13] Advances in additive manufacturing have furthered this potential by enabling the fabrication of LCNs in intricate shapes, a process often referred to as 4D printing due to the time-response nature of the 3D printed structures.[14–21] Therefore, azoLCNs show great promise as soft robotic actuators for a variety of actions including walking,[22] swimming,[23] jumping,[24–26] climbing,[27] and flying.[28] Several proof-of-concept devices have already been demonstrated, such as oscillators,[10,11,29] catapults,[24,30,31] microvalves,[32,33] grippers,[34–36] transporters,[37–39] and haptics.[40] Field applications ranging from nanoscale photonics to biomedical tools have been also posited.[41–43]

A potential advantage of liquid crystal polymers is in soft continuum robots,[44,45] because the material offers infinite, remotely addressable degrees of freedom.[46,47] However, the controllability of continuum robots so far, made by azoLCNs or any other materials, is either limited by the number of tethers or global stimulating fields, and few researchers have yet explored the large degrees of freedom of patterned optical stimuli to arbitrarily, reversibly, and dynamically control azoLCNs. Single variables such as optical polarization[48] and/or wavelength[1,49,50] were used in early demonstrations to control the bending direction of azoLCNs. Static preprogramming via domain patterning[51–54] can create optically actuated self-folding, complex structures by origami and kirigami.[55–57] However, domain patterning limits the azoLCN deformation to the shape dictated in the original design. Methods based on shape memory effect[30,35,58] and selective photocrosslinking[59] enable reconfigurable photoactuation, but require physical or chemical

E. R. Blackert, M. Barnes, H. Zhu
Department of Materials Science and NanoEngineering
Rice University
Houston, TX 77005, USA
E-mail: hanyu.zhu@rice.edu

P. Scaccia, V. Unhelkar
Department of Computer Science
Rice University
Houston, TX 77005, USA

T. M. S. K. Pathiranage, R. Verduzco
Department of Chemical and Biomolecular Engineering
Rice University
Houston, TX 77005, USA

The ORCID identification number(s) for the author(s) of this article can be found under https://doi.org/10.1002/aisy.202500045.

DOI: 10.1002/aisy.202500045

reprogramming.[58] In the prior demonstrations, the optical actuation was achieved by manually redirecting the entire light beam, which is a time-consuming and coarse mode of control. Meanwhile, structured light provides an avenue for more flexible, post-fabrication high-specificity control. For example, optical tweezers can control rotation and movement in micro- and nanoscale particles precisely with imaging-based feedback.[60] Spatially patterned light projections have been shown to cause localized bending and buckling in gold nanoparticle-based elastomers,[61–63] or selectively actuate among an array of azoLCNs.[21] Periodically scanned light pulses across azoLCN "caterpillars" or "slugs" can induce pulsating locomotion.[64,65] Yet highly adaptive, automated spatiotemporal optical control over azoLCN actuators has not been realized.

Here, we report the development a machine-learning-based, dynamic optical control method of an elastomeric azoLCN (azoLCE) soft robotic arm that enables multifunctionality without manual reprograming. The azoLCE was fabricated by a straightforward two-step polymerization method that results in an aligned monodomain sample. We projected the visible laser pattern, which can be rapidly altered by our control algorithm, on the robotic arm using a spatial light modulator (SLM). Each light spot dictated the point of bending along the azoLCE arm, the degree of bending and/or the amount of contraction, and the speed of response. Utilizing a convolutional neural network to learn the relation between light pattern and the resulting arm configuration, we inversely determined the input parameters required to achieve a desired shape. As a demonstration, we remotely manipulated a soft robotic arm to navigate around an obstacle. The platform described here realizes azoLCEs' capabilities for complex targeted motion and provides an important step toward tetherless azoLCN soft robotics with easily scalable material, actuation approach, and control model.[66–68]

2. Results and Discussion

The azoLCE arms were fabricated via two-stage thiol-acrylate polymerization and photocrosslinking.[69–71] Briefly, we first synthesized a hydroxyazo diacrylate (hereafter "azo") following the procedure described by Gelebart et al.[72] The azo derivative was selected for its ability to actuate to visible blue light with a center wavelength of 450 nm, which is beneficial for potential medical applications as opposed to cell-damaging UV light for actuating conventional azoLCEs, and for its short cis lifetime, which will allow the azoLCE to rapidly relax to its initial state after exposure. We combined the synthesized azo with reactive mesogen 257, a liquid crystal monomer chain extender; thiol linkers and crosslinkers; and eosin y and amine co-initiators, which respond to curing light with a longer wavelength center around 520 nm necessary to penetrate thick samples; all together in a chloroform solution. The mixture was dropcast in a Teflon mold for the first stage cure. The ratios of acrylates and thiols were controlled such that 15% excess acrylates remain. For the second stage, the material was stretched to approximately twice its initial length and cured under a green LED. This polymerized the excess acrylates and locks in the mechanical alignment and resulted in an azoLCE actuator of about $15 \times 4 \times 0.5$ mm with alignment along the long axis. For more details on azo synthesis and azoLCE fabrication, see Supporting Information.

To photoactuate the azoLCE with bidirectional bending, we set up two continuous wave 450 nm lasers on opposing optical paths as shown in **Figure 1**A. The two lasers are collimated prior to incidence on the left and right sides of the SLM screen, respectively. The SLM controls the phase field of each laser independently and diffracts the light energy into multiple directions, that is, beamlets with independently adjustable power toward the azoLCE (directed regions) or away from the azoLCE (Deflected beams) as shown in Figure 1B. The diffracted beams are then focused onto the sample's front and back surfaces by two lenses with 1000 mm focal length that form two areal patterns with adjustable shape and intensity. The azoLCE sample is then actuated by the intensity of light. The image in Figure 1A shows how the laser beams are split into beamlets that are spatially distributed along the azoLCE to achieve localized actuation. In order to control the actuating intensity on each bending joint independently, we must tune the intensity of each diffracted beam rather than the total laser power. To accomplish this, we use the SLM to split a certain portion of the light. The phase field at the SLM for generating the desired power distribution at the focal plane is calculated through a Gerchberg-Saxton algorithm. This technique is scalable from micrometer to meter size, because the field of view is simply proportional to the effective focal length of the lenses. To observe the azoLCE response, a camera is placed perpendicular to the optical path, with

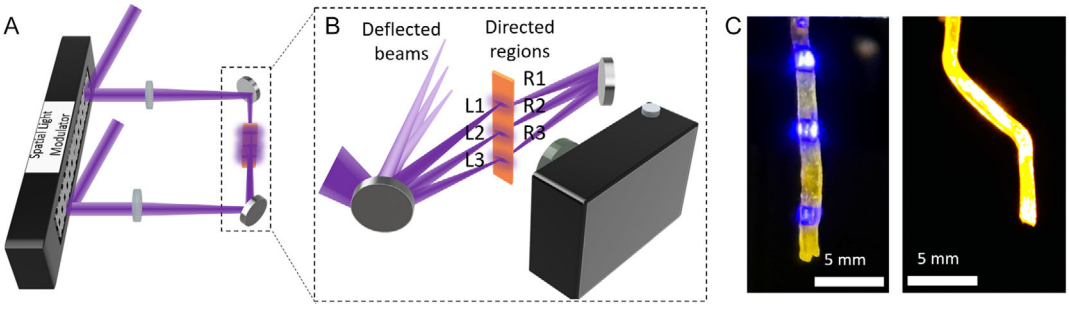

Figure 1. A) Schematic of a spatial light modulator directing two 450 nm lasers to various points on an azoLCE soft robot. B) Details of how laser power is distributed between deflected beams and directed regions to control the pattern and intensity of light on azoLCE. A camera is placed with a line of view perpendicular to the optical axis and the azoLCE arm to observe the sample's deformation. C) The camera images of the illumination pattern (left) and an example of AzoLCE bending in response to photoactuation (right, taken with a 585 nm bandpass filter).

a 585 nm bandpass filter to avoid excessive glare from the actuating lasers. In the example shown in Figure 1C, we achieve two distinct bending joints by changing the SLM phase to select two different laser patterns on the left and right optical paths. The azoLCE thermally relaxes back to the initial straight configuration after removing the laser illumination from the sample.

The azoLCE photoresponse is dependent on several variables, including the azoLCE chemistry, domain structure, and geometry, and the laser intensity, location, and focus spot(s).[48] In **Figure 2**A, we gained a better understanding of these dynamics for an azoLCE arm by plotting the displacement of the end effector, or tip, of the azoLCE, over time for various actuating intensities. For these tests, only the top "joint" of the azoLCE arm was actuated, allowing for the widest deflection distance as the entire arm swings left or right. At intensities less than ≈200 mW cm^{-2}, the azoLCE actuates and reaches an approximately steady-state displacement within about 10 s. The degree of displacement scales with intensity. Above this intensity threshold, the azoLCE actuates more rapidly. However, instead of reaching a steady state at the maximum displacement, the sample swings back to the center. This behavior can be attributed to photothermal heating of the sample. As the heat diffuses through the thickness of the azoLCE, we observe the contraction of the entire segment rather than a bending joint (Figure 2B). Within a short time of 3 s, such a heat transfer process is negligible for the purpose of controlling the sample geometry, as the displacement grows monotonically with incident laser power (Figure 2C). Within this timeframe, both photochemical and photothermal mechanisms contribute to the actuation.[8] Meanwhile, the photothermal transport dynamics becomes dominant if the laser pattern is held over 15 s, as a bending-to-shrinking transition can already be seen at intermediate power. The left inset image in Figure 2C shows a large bending displacement, while the right inset shows the segment contraction due to through-thickness thermal actuation. The time and intensity response are on the same order of magnitude as what has previously been reported for azo-based actuators.[37] Overall, the largest bending displacement occurring at any time saturates at about 200 mW cm^{-2}, beyond which an increase in power controls the length degree of freedom in addition to the curvature. Because we are interested in rapid and large actuation, we focused on the displacement versus intensity at 3 s. We select three intensities: 365, 200, and 37 mW cm^{-2} (above, at, and below the intensity threshold, respectively) for the following photoresponsive training.

For further photoresponse testing, we use the SLM to pattern light to three spots on each side of the azoLCE, as seen in Figure 1B (L1, L2, and L3 on the left and R1, R2, R3 on the right). Each photoactuated spot could be considered a transitory bending joint. It is important to note that, while we choose only a few joints for simplicity, the azoLCE actuator is in reality a continuum robot that can be actuated anywhere or everywhere. This is in contrast to previous studies which required predefined joints.[73] Since each side of the azoLCE is controlled by one laser, we cannot independently control the intensity of the spots by changing the power of the laser. Instead, we use the SLM to control what percentage of the laser power is directed toward the azoLCE. The total power of each laser is split among six regions—three on the azoLCE (directed regions) and three off of the azoLCE (deflected beams). Figure 1B also depicts this power splitting. Each directed region is composed of a row of three points, which keeps the Gerchberg–Saxton algorithm from becoming overly complex and allows us to maintain high diffraction efficiency while still actuating across the width of the azoLCE. The azoLCE response to the three horizontal spots is anticipated to be the same as one rectangle across the azoLCE with the same total power.[74]

Directing light toward three regions on each side of the azoLCE at three different powers, we tested 729 configurations (all permutations for three intensities per region, three regions per side, for two sides) and capture the azoLCE deformation after 3 s of illumination. An overlay of all 729 configurations is shown in **Figure 3**A, along with several examples in Figure 3B–G. The purple arrows on each image represent the actuating intensity for each corresponding joint. For example, in Figure 3C, the bottom left directed region (L3) is actuated at a high intensity of 365 mW cm^{-2}, resulting in a bend to the left at that point. Figure 3D primarily bends to the right in the center (R2) in response to actuation at that point. Notably, when a top joint is actuated with a high intensity such as R1 in Figure 3F, the sample is deflected such that the lowest directed region (L3) no longer hits the azoLCE. Samples were allowed 10 s to

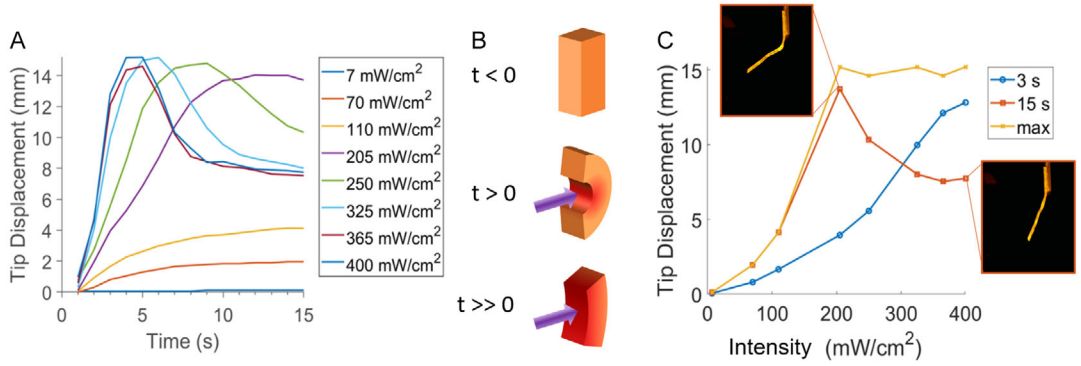

Figure 2. A) Displacement of the bottom tip of the azoLCE over time for various actuating intensities of 450 nm light focused on the top of the azoLCE. B) For high incident powers, as photoheating propagates into the sample from the surface, the illuminated azoLCE segment transits from bending to shrinking. C) Displacement of the azoLCE tip after 3 s, 15 s, and the maximum displacement (at any timepoint) as a function of actuating intensities. Insets: AzoLCE configuration at 15 s of actuation with 205 and 400 mW cm^{-2}, respectively.

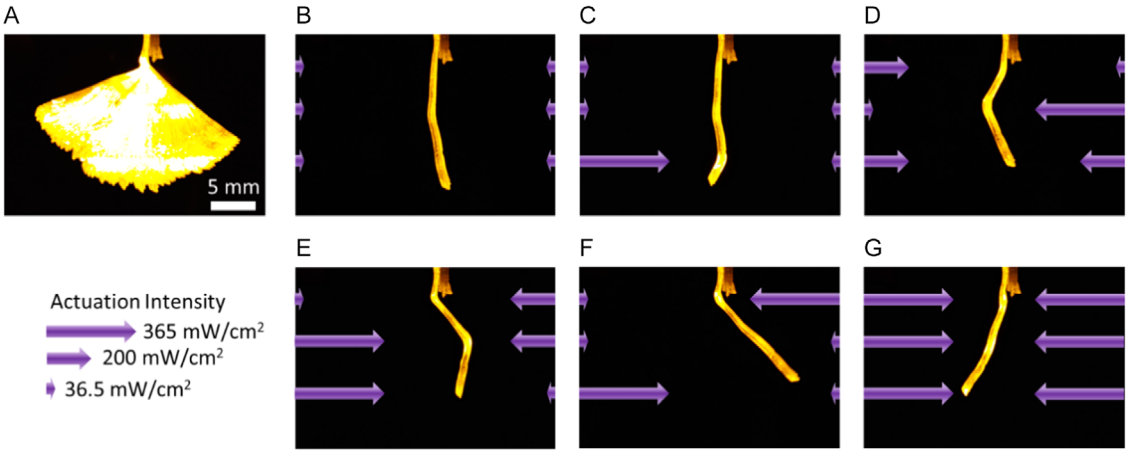

Figure 3. A) Overlay of actuation images demonstrating the actuation space of the azoLCE. B–G) AzoLCE configurations after three seconds of actuation. The purple arrows represent the actuating intensity incident on the azoLCE from the left and right at the three corresponding bending joints.

thermally relax before testing the next configuration. Figure 3G shows how the sample tends to contract rather than bend when actuated at a high intensity from both directions. Cumulatively, these results demonstrate the large actuation space and controllability of the azoLCE. While one could use these results to plan and direct azoLCE motions, it is preferable to automatically determine the necessary inputs for a desired azoLCE configuration. Predictions of azoLCE deformations have been demonstrated through first principal approaches to opto-mechanical modeling.[75,76] However, as a control method these models are limited by the accuracy of their baseline assumptions, which may vary based on fabrication, environment, and other factors. In contrast, machine learning-based approaches are highly adaptable to the complex, nonlinear dynamics of soft robots without requiring explicit, detailed modeling of their variable behaviors. Previously, Almanzor et al. demonstrated the training and use of an image-based neural network to control the configuration of a pneumatic soft robot.[77] Here we take a similar approach to develop an image-based neural network to control the configuration of the azoLCE arm.

To achieve arbitrary arm configurations, we used the collected azoLCE deformation images to train a basic convolutional neural network (CNN), a common machine learning tool widely employed for image-based object detection and motion planning.[78,79] The structure of our CNN for detecting the action of a single arm is shown in **Figure 4**A, built using Tensorflow with the Keras library in Python. The input images (scaled down to 35 × 35 pixels in normalized grayscale) are represented as 2D numpy arrays and the outputs are six laser power levels between 0 and 1 (for 0% to 100% of the laser light being directed toward the azoLCE for the corresponding spot). To extract features such as edges and curvatures, we applied 32 3 × 3-pixel filters in the CNN. The resulting intermediate 33 × 33 × 32 tensor is subsequently flattened into a 1D array and connected through one hidden dense layer with 100 nodes to the final output layer with 6 parameters of laser power output at each location. The CNN was trained on the dataset consisting of 729 laser power settings and the corresponding experimentally observed arm configurations and optimized using stochastic gradient descent with a learning rate of 0.01. While the training data was limited to three power levels for each spot (0.1, 0.5, or 1), the CNN is not constrained, and the outputs can be any intensity within this range. After the training, we validated the CNN by inputting casually drawn linear configurations as the goal of arm configuration, obtaining the output laser parameters from the CNN, and then experimentally applying the laser parameters to observe the arm's responses. For example, in Figure 4B, we show the as-drawn configuration. The CNN outputs the following relative powers, normalized to the maximum of 365 mW cm^{-2}: 0.04, 0.99, 0.32, 0.98, 0.68, and 0.99 for the 6 laser illumination regions L1-R3. These values

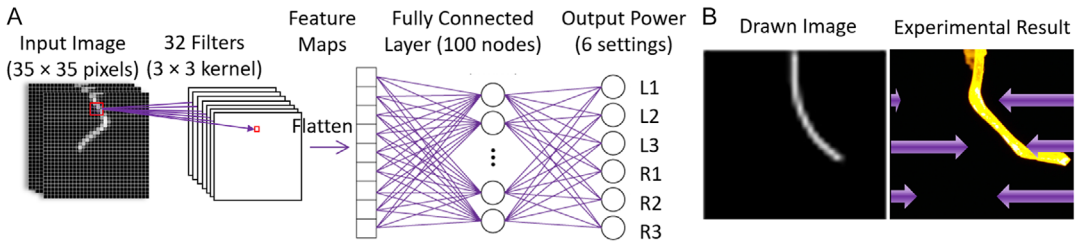

Figure 4. A) The convolutional neural network structure was trained on experimental images of the azoLCE configurations with the corresponding laser power settings. The input compressed images were first filtered to create feature maps and then connected through a hidden layer to the output settings. B) The trained CNN was tested with a hand-drawn azoLCE configuration as the goal (left) and predicted the corresponding laser power levels. We then experimentally applied the power settings and found that the resulting geometry (right) agrees well with the drawing.

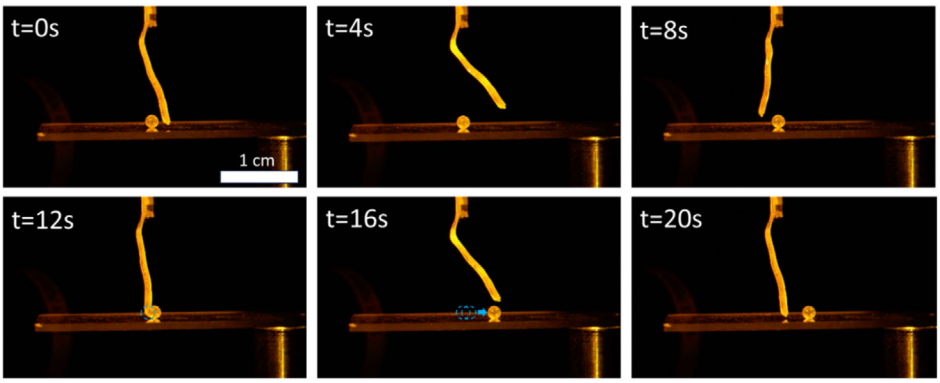

Figure 5. An azoLCE circumvents a small ball and then pushes the ball across a glass slide.

correspond to 14.6, 361, 116.8, 358, 248, and 361 mW cm^{-2} on the azoLCE, respectively. We calculate the necessary phase hologram and use the SLM to direct these powers to the azoLCE and capture an image, Figure 4B (right), of the resulting deformation after 3 s of illumination. Evidently, the resulting azoLCE response is close to the desired configuration. This initial test shows the promising capability of neural network-informed optical field control of azoLCEs for soft robotic applications.

With the capability of automating the input control parameters, it becomes easier to direct the azoLCE to perform complex actions. To demonstrate this, we directed the azoLCE to kick a soccer ball, that is, moving up and around a small obstacle before striking it from the back. **Figure 5** shows the azoLCE at several timepoints during this process, as extracted from a video available in the Supporting Information. At $t = 0$ s, the azoLCE is in a relaxed configuration with a small ball adjacent to the left. At $t = 4$ s, actuation on the right side causes the azoLCE to bend to the right. By quickly switching from right to left actuation, the azoLCE remains contracted while in motion and avoids hitting the ball ($t = 8$ s). The azoLCE is then in position to nudge the ball to the right ($t = 12$ s). Next, the azoLCE is actuated once again from the right side, which results in nudging the ball to the right ($t = 16$ s). Finally, the azoLCE relaxes to its initial configuration, now with the ball on its right ($t = 20$ s). This action would be difficult to perform without light modulation and slow to direct manually. The neural network optical control scheme facilitates quick reconfiguration of the azoLCE arm.

Future work may introduce a second camera to track and control the out-of-plane deformation of the azoLCE arm to realize a truly 3D motional space. With further developments in image-correlated feedback, this platform could further be improved in terms of speed and fidelity. For instance, dynamic laser targeting could account for azoLCE movements so that multiple joints are still achievable even when the highest joint causes large deflection. The infrastructure described here is in principle scalable by introducing more complex CNN models for controlling multiple interacting objects with hundreds of diffracted laser beamlets allowed by a single SLM. Additionally, recent advancements in spatiotemporal focusing[53] and higher order optical processes for 3D printing[16] can be extended to 4D printing control azoLCNs in time. The electronic asymmetry of a hydroxy-substituted azo potentially enables two-photon actuation, which would allow for single-beam volumetric control with biologically friendly infrared light.[80]

3. Conclusion

In summary, we have demonstrated high-dimensional, spatiotemporal optical control of azoLCEs without the need for preprogrammed domain configurations. Unique from previous demonstrations of photoactuation, we realized multiple independent and simultaneously maneuverable bending joints in the same robotic arm. The bending joints can be arbitrarily selected by the structured light pattern and are not constrained by preprogrammed domains. Future work will be to expand this control scheme to realize 3D robotic configurations beyond those described here, such as out-of-pane bending, with a second camera as feedback. A convolutional neural network was trained and tested, enabling rapid determination of required patterns to achieve a desired configuration. Our work paves the way for remotely powered and maneuvered soft robots for photomechanical and biomedical applications.

Supporting Information

Supporting Information is available from the Wiley Online Library or from the author.

Acknowledgements

H.Z. is supported by the US National Science Foundation (NSF) under award number DMR-2240106. E.B. is supported by the Graduate Research Fellowship Program (GRFP) from the US National Science Foundation (NSF) under grant number DGE-1842494 and the NSF Research Traineeship Award under grant number 1828869. M.B., T.P., and R.V. acknowledge the support of the Welch Foundation C-2124 and Army Research Office Chemical Sciences Division W911NF1810289. V.U. acknowledges the support of Rice University funds. The authors thank Dr. Yifan Zhu for the helpful discussion and support regarding photocrosslinkers.

Conflict of Interest

The authors declare no conflict of interest.

Author Contributions

Elizabeth R. Blackert: conceptualization (equal); data curation (equal); investigation (lead); methodology (lead); software (supporting); validation (lead); visualization (lead); writing—original draft (lead); writing—review and editing (lead). **Phoebe Scaccia**: investigation (supporting); software (lead); visualization (supporting); writing—review and editing (supporting). **Morgan Barnes**: investigation (supporting); methodology (supporting); validation (supporting); writing—review and editing (supporting). **Taniya M. S. K. Pathiranage**: methodology (supporting); validation (supporting); visualization (supporting); writing—review and editing (supporting). **Rafael Verduzco**: funding acquisition (supporting); methodology (supporting); resources (supporting); supervision (supporting); writing—review and editing (supporting). **Vaibhav Unhelkar**: methodology (supporting); software (supporting); validation (supporting); writing—review and editing (supporting). **Hanyu Zhu**: conceptualization (lead); data curation (equal); funding acquisition (lead); investigation (equal); methodology (equal); project administration (lead); supervision (lead); validation (lead); visualization (supporting); writing—original draft (equal); writing—review and editing (equal).

Data Availability Statement

The data that support the findings of this study are available from the corresponding author upon reasonable request.

Keywords

azobenzene, convolutional neural networks, dynamical optical patterning, liquid crystal elastomers, robotics

Received: February 25, 2025
Published online:

[1] Y. Yu, M. Nakano, T. Ikeda, *Nature* **2003**, *425*, 2003.
[2] H. Koerner, T. J. White, N. V. Tabiryan, T. J. Bunning, R. A. Vaia, *Mater. Today* **2008**, *11*, 34.
[3] T. J. White, *J. Polym. Sci., Part B: Polym. Phys.* **2018**, *56*, 695.
[4] A. S. Kuenstler, R. C. Hayward, *Curr. Opin. Colloid Interface Sci.* **2019**, *40*, 70.
[5] L. Qin, X. Liu, Y. Yu, *Adv. Opt. Mater.* **2021**, *9*, 2001743.
[6] J. Hu, M. Yu, M. Wang, K.-L. Choy, H. Yu, *ACS Appl. Mater. Interfaces* **2022**, *14*, 12951.
[7] S. Kong, H. Wang, E. Ubba, Y. Xiao, T. Yu, W. Huang, *Research* **2023**, *6*, 0242.
[8] K. M. Lee, T. J. White, *Macromolecules* **2012**, *45*, 7163.
[9] M. Pilz Da Cunha, E. A. J. van Thoor, M. G. Debije, D. J. Broer, A. P. H. J. Schenning, *J. Mater. Chem. C* **2019**, *7*, 13502.
[10] T. J. White, N. V. Tabiryan, S. V. Serak, U. A. Hrozhyk, V. P. Tondiglia, H. Koerner, A. Vaia, T. J. Bunning, *Soft Matter* **2008**, *4*, 1796.
[11] S. Serak, N. Tabiryan, R. Vergara, T. J. White, R. A. Vaia, T. J. Bunning, *Soft Matter* **2010**, *6*, 779.
[12] M. Kondo, R. Miyasato, Y. Naka, J. I. Mamiya, M. Kinoshita, Y. Yu, C. J. Barrett, T. Ikeda, *Liq. Cryst.* **2009**, *36*, 1289.
[13] S. Li, M. M. Lerch, J. T. Waters, B. Deng, R. S. Martens, Y. Yao, D. Y. Kim, K. Bertoldi, A. Grinthal, A. C. Balazs, J. Aizenberg, *Nature* **2022**, *605*, 76.
[14] C. D. P. Cerbuna, *Mechanically Responsive Materials for Soft Robotics* (Ed: H. Koshima), Wiley-VCH Verlag GmbH & Co, KGaA, Weinheim **2020**, pp. 347–362.
[15] M. Barnes, S. M. Sajadi, S. Parekh, M. M. Rahman, P. M. Ajayan, R. Verduzco, *ACS Appl. Mater. Interfaces* **2020**, *12*, 28692.
[16] P. Somers, Z. Liang, J. E. Johnson, B. W. Boudouris, L. Pan, X. Xu, *Light Sci. Appl.* **2021**, *10*, 199.
[17] A. Münchinger, V. Hahn, D. Beutel, S. Woska, J. Monti, C. Rockstuhl, E. Blasco, M. Wegener, *Adv. Mater. Technol.* **2022**, *7*, 2100944.
[18] L. Ceamanos, D. J. Mulder, Z. Kahveci, M. López-Valdeolivas, A. P. H. J. Schenning, C. Sánchez-Somolinos, *J. Mater. Chem. B* **2023**, *11*, 4083.
[19] L. McDougall, J. Herman, E. Huntley, S. Leguizamon, A. Cook, T. White, B. Kaehr, D. J. Roach, *ACS Appl. Mater. Interfaces* **2023**, *15*, 58897.
[20] M. Chen, Y. Hou, R. An, H. J. Qi, K. Zhou, *Adv. Mater.* **2024**, *36*, 2303969.
[21] Y. Wang, J. Qian, *Sens. Actuators, A* **2024**, *368*, 115142.
[22] H. Zeng, P. Wasylczyk, C. Parmeggiani, D. Martella, M. Burresi, D. S. Wiersma, *Adv. Mater.* **2015**, *27*, 3883.
[23] M. Camacho-Lopez, H. Finkelmann, P. Palffy-Muhoray, M. Shelley, *Nat. Mater.* **2004**, *3*, 307.
[24] H. Guo, A. Priimagi, H. Zeng, *Adv. Funct. Mater.* **2022**, *32*, 2108919.
[25] T. S. Hebner, K. Korner, C. N. Bowman, K. Bhattacharya, T. J. White, *Sci. Adv.* **2023**, *9*, eade1320.
[26] B. Lei, Z.-Y. Wen, H.-K. Wang, J. Gao, L.-J. Chen, *ACS Appl. Mater. Interfaces* **2024**, *16*, 1596.
[27] J. Sun, L. Bauman, L. Yu, B. Zhao, *Cell Rep. Phys. Sci.* **2023**, *4*, 101241.
[28] T. Song, H. Lei, A. J. Clancy, S. Ma, H. Yu, L. Zhang, *Nano Energy* **2021**, *87*, 106207.
[29] M. Pilz da Cunha, A. R. Peeketi, A. Ramgopal, R. K. Annabattula, A. P. H. J. Schenning, *ChemistryOpen* **2020**, *9*, 1149.
[30] K. M. Lee, H. Koerner, R. A. Vaia, T. J. Bunning, T. J. White, *Soft Matter* **2011**, *7*, 4318.
[31] B. Lei, H.-K. Wang, K.-H. Wu, J. Gao, L.-J. Chen, *Adv. Intell. Syst.* **2023**, *5*, 2200360.
[32] M. Chen, H. Huang, Y. Zhu, Z. Liu, X. Xing, F. Cheng, Y. Yu, *Appl. Phys. A* **2011**, *102*, 667.
[33] J. Lv, Y. Liu, J. Wei, E. Chen, L. Qin, Y. Yu, *Nature* **2016**, *537*, 179.
[34] F. Cheng, R. Yin, Y. Zhang, C.-C. Yen, Y. Yu, *Soft Matter* **2010**, *6*, 3447.
[35] M. Lahikainen, H. Zeng, A. Priimagi, *Nat. Commun.* **2018**, *9*, 4148.
[36] M. Pilz da Cunha, Y. Foelen, R. J. H. van Raak, J. N. Murphy, T. A. P. Engels, M. G. Debije, A. P. H. J. Schenning, *Adv. Opt. Mater.* **2019**, *7*, 1801643.
[37] M. Pilz da Cunha, S. Ambergen, M. G. Debije, E. F. G. A. Homburg, J. M. J. den Toonder, A. P. H. J. Schenning, *Adv. Sci.* **2020**, *7*, 1902842.
[38] Y. Zhu, L. Zheng, Z. Liu, H. Liu, Y. Yu, *Appl. Phys. A* **2014**, *115*, 1167.
[39] N. Qian, H. K. Bisoyi, M. Wang, S. Huang, Z. Liu, X.-M. Chen, J. Hu, H. Yang, Q. Li, *Adv. Funct. Mater.* **2023**, *33*, 2214205.
[40] N. Torras, K. E. Zinoviev, C. J. Camargo, E. M. Campo, H. Campanella, J. Esteve, J. E. Marshall, E. M. Terentjev, M. Omastová, I. Krupa, P. Teplický, B. Mamojka, P. Bruns, B. Roeder, M. Vallribera, R. Malet, S. Zuffanelli, V. Soler, J. Roig, N. Walker, D. Wenn, F. Vossen, F. M. H. Crompvoets, *Sens. Actuators, A* **2014**, *208*, 104.
[41] H. Yu, *J. Mater. Chem. C* **2014**, *2*, 3047.
[42] A. Kirillova, L. Ionov, *J. Mater. Chem. B* **2019**, *7*, 1597.
[43] M. Li, A. Pal, A. Aghakhani, A. Pena-Francesch, M. Sitti, *Nat. Rev. Mater.* **2022**, *7*, 235.
[44] M. Russo, S. M. H. Sadati, X. Dong, A. Mohammad, I. D. Walker, C. Bergeles, K. Xu, D. A. Axinte, *Adv. Intell. Syst.* **2023**, *5*, 2200367.
[45] J. Burgner-Kahrs, D. C. Rucker, H. Choset, *IEEE Trans. Robot.* **2015**, *31*, 1261.
[46] Y. Guo, J. Zhang, W. Hu, M. T. A. Khan, M. Sitti, *Nat. Commun.* **2021**, *12*, 5936.
[47] S. Li, H. Bai, Z. Liu, X. Zhang, C. Huang, L. W. Wiesner, M. Silberstein, R. F. Shepherd, *Sci. Adv.* **2021**, *7*, eabg3677.

[48] T. J. White, S. V. Serak, N. V. Tabiryan, R. A. Vaiaa, T. J. Bunning, *J. Mater. Chem.* **2008**, *19*, 1080.
[49] M. Yamada, M. Kondo, J. Mamiya, Y. Yu, M. Kinoshita, C. J. Barrett, T. Ikeda, *Angew. Chem.* **2008**, *120*, 5064.
[50] J.-H. Yun, C. Li, S. Kim, M. Cho, *J. Phys. Chem. C* **2018**, *122*, 6310.
[51] V. P. Tondiglia, T. J. White, *Science* **2015**, *347*, 982.
[52] J. J. Wie, M. R. Shankar, T. J. White, *Nat. Commun.* **2016**, *7*, 13260.
[53] Y. Guo, M. Jiang, C. Peng, K. Sun, O. Yaroshchuk, O. Lavrentovich, Q.-H. Wei, *Adv. Mater.* **2016**, *28*, 2353.
[54] M. Javed, T. Corazao, M. O. Saed, C. P. Ambulo, Y. Li, M. R. Kessler, T. H. Ware, *ACS Appl. Mater. Interfaces* **2022**, *14*, 35087.
[55] J. Ryu, M. D'Amato, X. Cui, K. N. Long, H. Jerry Qi, M. L. Dunn, *Appl. Phys. Lett.* **2012**, *100*, 161908.
[56] J. Chen, A. S. Johnson, J. Weber, O. I. Akomolafe, J. Jiang, C. Peng, *Adv. Intell. Syst.* **2022**, *4*, 2100233.
[57] J. Chen, J. Jiang, J. Weber, V. Gimenez-Pinto, C. Peng, *ACS Appl. Mater. Interfaces* **2023**, *15*, 4538.
[58] D. Iqbal, M. H. Samiullah, *Materials* **2013**, *6*, 116.
[59] C. Valenzuela, Y. Chen, L. Wang, W. Feng, *Chem. Euro. J.* **2022**, *28*, e202201957.
[60] X. Chen, Y. Zhao, Y. Zhang, B. Li, Y. Li, L. Jiang, *Small Methods* **2024**, *8*, 2301105.
[61] Y. Sun, J. S. Evans, T. Lee, B. Senyuk, P. Keller, S. He, I. I. Smalyukh, *Appl. Phys. Lett.* **2012**, *100*, 241901.
[62] A. W. Hauser, D. Liu, K. C. Bryson, R. C. Hayward, D. J. Broer, *Macromolecules* **2016**, *49*, 1575.
[63] V. M. Kryshenik, Y. M. Azhniuk, V. S. Kovtunenko, *J. Non-Cryst. Solids* **2019**, *512*, 112.
[64] S. Palagi, A. G. Mark, S. Y. Reigh, K. Melde, T. Qiu, H. Zeng, C. Parmeggiani, D. Martella, A. Sanchez-Castillo, N. Kapernaum, F. Giesselmann, D. S. Wiersma, E. Lauga, P. Fischer, *Nat. Mater.* **2016**, *15*, 647.
[65] M. Rogóż, H. Zeng, C. Xuan, D. S. Wiersma, P. Wasylczyk, *Adv. Opt. Mater.* **2016**, *4*, 1689.
[66] M. Sitti, D. S. Wiersma, *Adv. Mater.* **2020**, *32*, 1906766.
[67] S. Huang, Y. Huang, Q. Li, *Small Struct.* **2021**, *2*, 2100038.
[68] M. Rogóż, Z. Dziekan, K. Dradrach, M. Zmyślony, P. Nałęcz-Jawecki, P. Grabowski, B. Fabjanowicz, M. Podgórska, A. Kudzia, P. Wasylczyk, *Materials* **2022**, *15*, 8214.
[69] J. Kupfer, H. Finkelmann, *Makromol. Chem.* **1991**, *12*, 717.
[70] C. M. Yakacki, M. Saed, D. P. Nair, T. Gong, S. M. Reed, C. N. Bowman, *RSC Adv.* **2015**, *5*, 18997.
[71] M. Barnes, R. Verduzco, *Soft Matter* **2019**, *15*, 870.
[72] A. H. Gelebart, D. J. Mulder, M. Varga, A. Konya, G. Vantomme, *Nature* **2017**, *546*, 632.
[73] M. Liu, Q. Wang, A.-W. Li, H.-B. Sun, *Phys. Chem. Chem. Phys.* **2023**, *25*, 9753.
[74] P. Grabowski, J. Haberko, P. Wasylczyk, *Materials* **2020**, *13*, 2933.
[75] L. Liu, P. R. Onck, *Soft Matter* **2018**, *14*, 2411.
[76] W. M. van Rees, E. Vouga, L. Mahadevan, *Proc. Natl. Acad. Sci.* **2017**, *114*, 11597.
[77] E. Almanzor, F. Ye, J. Shi, T. G. Thuruthel, H. A. Wurdemann, F. Iida, *IEEE Trans. Robot.* **2023**, *39*, 2973.
[78] A. Dhillon, G. K. Verma, *Prog. Artif. Intell.* **2020**, *9*, 85.
[79] C. Zhou, B. Huang, P. Fränti, *J. Intell. Manuf.* **2022**, *33*, 387.
[80] S. Pearson, J. Feng, A. del Campo, *Adv. Funct. Mater.* **2021**, *31*, 2105989.